

# Inclusive pion and eta production in p+Nb collisions at 3.5 GeV beam energy

G. Agakishiev<sup>7</sup>, A. Balanda<sup>3</sup>, D. Belver<sup>18</sup>, A. Belyaev<sup>7</sup>, J.C. Berger-Chen<sup>9</sup>, A. Blanco<sup>2</sup>, M. Böhmer<sup>10</sup>, J. L. Boyard<sup>16</sup>, P. Cabanelas<sup>18</sup>, S. Chernenko<sup>7</sup>, A. Dybczak<sup>3</sup>, E. Epple<sup>9</sup>, L. Fabbietti<sup>9</sup>, O. Fateev<sup>7</sup>, P. Finocchiaro<sup>1</sup>, P. Fonte<sup>2,b</sup>, J. Friese<sup>10</sup>, I. Fröhlich<sup>8</sup>, T. Galatyuk<sup>5,c</sup>, J. A. Garzón<sup>18</sup>, R. Gernhäuser<sup>10</sup>, K. Göbel<sup>8</sup>, M. Golubeva<sup>13</sup>, D. González-Díaz<sup>5</sup>, F. Guber<sup>13</sup>, M. Gumberidze<sup>5,16,\*</sup>, T. Heinz<sup>4</sup>, T. Hennino<sup>16</sup>, R. Holzmann<sup>4,\*</sup>, A. Ierusalimov<sup>7</sup>, I. Iori<sup>12,e</sup>, A. Ivashkin<sup>13</sup>, M. Jurkovic<sup>10</sup>, B. Kämpfer<sup>6,d</sup>, T. Karavicheva<sup>13</sup>, I. Koenig<sup>4</sup>, W. Koenig<sup>4</sup>, B. W. Kolb<sup>4</sup>, G. Kornakov<sup>18</sup>, R. Kotte<sup>6</sup>, A. Krása<sup>17</sup>, F. Krizek<sup>17</sup>, R. Krücken<sup>10</sup>, H. Kuc<sup>3,16</sup>, W. Kühn<sup>11</sup>, A. Kugler<sup>17</sup>, A. Kurepin<sup>13</sup>, V. Ladygin<sup>7</sup>, R. Lalik<sup>9</sup>, S. Lang<sup>4</sup>, K. Lapidus<sup>9</sup>, A. Lebedev<sup>14</sup>, T. Liu<sup>16</sup>, L. Lopes<sup>2</sup>, M. Lorenz<sup>8,c</sup>, L. Maier<sup>10</sup>, A. Mangiarotti<sup>2</sup>, J. Markert<sup>8</sup>, V. Metag<sup>11</sup>, B. Michalska<sup>3</sup>, J. Michel<sup>8</sup>, C. Müntz<sup>8</sup>, L. Naumann<sup>6</sup>, Y. C. Pachmayer<sup>8</sup>, M. Palka<sup>3</sup>, Y. Parpottas<sup>15,f</sup>, V. Pechenov<sup>4</sup>, O. Pechenova<sup>8</sup>, J. Pietraszko<sup>4</sup>, W. Przygoda<sup>3</sup>, B. Ramstein<sup>16</sup>, A. Reshetin<sup>13</sup>, A. Rustamov<sup>8</sup>, A. Sadovsky<sup>13</sup>, P. Salabura<sup>3</sup>, A. Schmah<sup>9,a</sup>, E. Schwab<sup>4</sup>, J. Siebenson<sup>9</sup>, Yu.G. Sobolev<sup>17</sup>, S. Spataro<sup>11,g</sup>, B. Spruck<sup>11</sup>, H. Ströbele<sup>8</sup>, J. Stroth<sup>8,4</sup>, C. Sturm<sup>4</sup>, A. Tarantola<sup>8</sup>, K. Teilab<sup>8</sup>, P. Tlustý<sup>17</sup>, M. Traxler<sup>4</sup>, R. Trebacz<sup>3</sup>, H. Tsertos<sup>15</sup>, T. Vasiliev<sup>7</sup>, V. Wagner<sup>17</sup>, M. Weber<sup>10</sup>, C. Wendisch<sup>6,d</sup>, J. Wüstenfeld<sup>6</sup>, S. Yurevich<sup>4</sup>, Y. Zanevsky<sup>7</sup>

(HADES collaboration)

<sup>1</sup>*Istituto Nazionale di Fisica Nucleare - Laboratori Nazionali del Sud, 95125 Catania, Italy*

<sup>2</sup>*LIP-Laboratório de Instrumentação e Física Experimental de Partículas, 3004-516 Coimbra, Portugal*

<sup>3</sup>*Smoluchowski Institute of Physics, Jagiellonian University of Cracow, 30-059 Kraków, Poland*

<sup>4</sup>*GSI Helmholtzzentrum für Schwerionenforschung GmbH, 64291 Darmstadt, Germany*

<sup>5</sup>*Technische Universität Darmstadt, 64289 Darmstadt, Germany*

<sup>6</sup>*Institut für Strahlenphysik, Helmholtz-Zentrum Dresden-Rossendorf, 01314 Dresden, Germany*

<sup>7</sup>*Joint Institute of Nuclear Research, 141980 Dubna, Russia*

<sup>8</sup>*Institut für Kernphysik, Goethe-Universität, 60438 Frankfurt, Germany*

<sup>9</sup>*Excellence Cluster 'Origin and Structure of the Universe', 85748 Garching, Germany*

<sup>10</sup>*Physik Department E12, Technische Universität München, 85748 Garching, Germany*

<sup>11</sup>*II. Physikalisches Institut, Justus Liebig Universität Giessen, 35392 Giessen, Germany*

<sup>12</sup>*Istituto Nazionale di Fisica Nucleare, Sezione di Milano, 20133 Milano, Italy*

<sup>13</sup>*Institute for Nuclear Research, Russian Academy of Science, 117312 Moscow, Russia*

<sup>14</sup>*Institute of Theoretical and Experimental Physics, 117218 Moscow, Russia*

<sup>15</sup>*Department of Physics, University of Cyprus, 1678 Nicosia, Cyprus*

<sup>16</sup>*Institut de Physique Nucléaire (UMR 8608), CNRS/IN2P3 - Université Paris Sud, F-91406 Orsay Cedex, France*

<sup>17</sup>*Nuclear Physics Institute, Academy of Sciences of Czech Republic, 25068 Rez, Czech Republic*

<sup>18</sup>*LabCAF. F. Física, Univ. de Santiago de Compostela, 15706 Santiago de Compostela, Spain*

<sup>a</sup> *now at Lawrence Berkeley National Laboratory, Berkeley, USA*

<sup>b</sup> *also at ISEC Coimbra, Coimbra, Portugal*

<sup>c</sup> *also at ExtreMe Matter Institute EMMI, 64291 Darmstadt, Germany*

<sup>d</sup> *also at Technische Universität Dresden, 01062 Dresden, Germany*

<sup>e</sup> *also at Dipartimento di Fisica, Università di Milano, 20133 Milano, Italy*

<sup>f</sup> *also at Frederick University, 1036 Nicosia, Cyprus*

<sup>g</sup> *now at Dipartimento di Fisica Generale and INFN, Università di Torino, 10125 Torino, Italy*

\* *Corresponding authors: R.Holzmann@gsi.de, M.Gumberidze@gsi.de*

(Dated: July 8, 2013)

Data on inclusive pion and eta production measured with the dielectron spectrometer HADES in the reaction p+<sup>93</sup>Nb at a kinetic beam energy of 3.5 GeV are presented. Our results, obtained with the photon-conversion method, supplement the rather sparse information on neutral-meson production in proton-nucleus reactions existing for this bombarding energy regime. The reconstructed e<sup>+</sup>e<sup>-</sup>e<sup>+</sup>e<sup>-</sup> transverse-momentum and rapidity distributions are confronted with transport-model calculations, which account fairly well for both  $\pi^0$  and  $\eta$  production.

PACS numbers: 25.40.Ep, 13.40.Hq

## I. INTRODUCTION

The High-Acceptance DiElectron Spectrometer (HADES) experiment at GSI pursues a comprehensive program of dielectron emission studies in few-GeV

nucleon-nucleon [1, 2], proton-nucleus [3], and nucleus-nucleus collisions [4]. Dilepton spectroscopy allows to investigate the properties of hadrons produced, propagated, and decayed in a strongly interacting medium. This is because leptons (electrons and muons)

do not themselves interact strongly when traveling through finite-sized hadronic matter, that is, their kinematics remain basically undistorted. Lepton-pair measurements are hence ideally suited to search for medium modifications of hadrons in nuclear matter [5, 6]. The observed dilepton spectra consist, however, of a complex superposition of various mesonic and baryonic contributions, and their interpretation requires a detailed knowledge of all sources. Indeed, early interpretations of dilepton spectra from relativistic heavy-ion collisions commonly introduced a schematic distinction of (i) hard initial contributions related to Drell-Yan type processes, (ii) the thermal radiation off the fireball, and (iii) the hadronic cocktail from late decays following its disassembly (cf. [7]). Transport models supersede this artificial separation as they describe all phases of the collision on an equal footing by following continuously virtual and real photon emission over time. Presently, they are commonly employed in the few-GeV bombarding energy regime to describe particle production and propagation through the medium, in particular, when dealing with the complex dynamics of nucleus-nucleus reactions [8–13]. Comprehensive information on meson production is thereby mandatory to benchmark and constrain those calculations. In this context the neutral pion and eta mesons are of particular interest as they contribute largely to the dilepton spectrum via their Dalitz decays,  $\pi^0 \rightarrow \gamma\gamma^* \rightarrow \gamma e^+e^-$  and  $\eta \rightarrow \gamma\gamma^* \rightarrow \gamma e^+e^-$ , respectively.

Although in the few-GeV energy regime a large body of systematic data on pion and, to a lesser extent, on eta production in nucleus-nucleus collisions has been gathered over the last decades, mostly at the Bevalac, the AGS, and SIS18 accelerators, there is much less information available from proton-nucleus reactions. The latter ones are, however, important as an intermediate step between nucleon-nucleon and nucleus-nucleus collisions. Charged pions from p+A have been measured at the Bevalac with proton beams of kinetic energies up to 2.1 GeV [14], at TRIUMF up to 0.5 GeV [15], and recently by the HARP experiment at the CERN PS with proton energies between 2 and 12 GeV [16]. Information on eta production in p+A reactions is even more scarce. Only the PINOT experiment at the SATURNE accelerator in Saclay provided data for proton energies in the range of 0.8 – 1.5 GeV [17].

In this paper we supplement the available body of experimental results on pion ( $\pi^0, \pi^-$ ) and eta production in p+A collisions with data obtained with HADES in the p+Nb reaction at 3.5 GeV. Negative pions have been identified via their characteristic energy loss vs. momentum signature in the HADES time-of-flight (TOF) system. The neutral mesons,  $\pi^0$  and  $\eta$ , were reconstructed with the photon-conversion technique in which meson decay photons are detected via their external conversion into an  $e^+e^-$  pair via a Bethe-Heitler process, preferentially in high- $Z$  materials. This method has been developed foremost in high-energy physics experiments

[18–22] to study the radiative decays of the quarkonium states  $\chi_c$  into  $J/\Psi + \gamma$  and  $\chi_b$  into  $\Upsilon + \gamma$ . It has also been used in high-energy heavy-ion reactions, namely by the PHENIX experiment at RHIC, studying Au+Au collisions at a nucleon-nucleon center-of-mass energy of  $\sqrt{s_{NN}} = 200$  GeV [23] and by the ALICE experiment at the LHC in  $\sqrt{s_{NN}} = 7$  TeV p+p collisions [24]. Making use of the good momentum resolution of charged-particle trackers, in particular at low energies, the conversion technique offers typically better energy resolution than a photon calorimeter. We demonstrate here the applicability of the method with HADES in few-GeV reactions.

Our paper is organized as follows. Section II describes the experiment and the employed particle identification procedures. In Sec. III the photon-conversion method is introduced. Pion and eta spectra, as well as meson multiplicities are presented in Sec. IV. In Sec. V we compare the data with transport-model calculations and, finally, in Sec. VI we summarize our findings. A preliminary version of the  $\pi^-$  data shown here has already been presented elsewhere [25].

## II. THE EXPERIMENT

The six-sector high-acceptance spectrometer HADES operates at the GSI Helmholtzzentrum für Schwerionenforschung in Darmstadt where it takes beams from the heavy-ion synchrotron SIS18. Although its setup was originally optimized for dielectron spectroscopy, HADES is in fact a versatile charged-particle detector with both good efficiency and momentum resolution. Its main component serving for electron and positron selection is a hadron-blind Ring-Imaging Cherenkov detector (RICH). Further particle identification power is provided by the time of flight measured in a plastic scintillator TOF wall, the electromagnetic shower characteristics observed in a pre-shower detector, and the energy-loss signals from the scintillators of the TOF wall as well as from the four planes of drift chambers serving as tracking stations. Charged particles are tracked through a toroidal magnetic field provided by a six-coil iron-less superconducting magnet. All technical aspects of the detector are described in [26].

In the experiment discussed here a proton beam with a kinetic energy of  $E_p = 3.5$  GeV and an average intensity of about  $2 \times 10^6$  particles per second impinged onto a 12-fold segmented niobium ( $^{93}\text{Nb}$ ) target with a total thickness of 5.4 mm and corresponding to 2.8% nuclear interaction probability. The online event selection was done in two steps: a 1<sup>st</sup>-level trigger (LVL1) selected events with at least three charged-particle hits in the TOF wall ( $N_{ch} \geq 3$ ) and a 2<sup>nd</sup>-level trigger (LVL2) fired if an electron or positron candidate was recognized. While all LVL2 events were recorded, the LVL1-only events were downscaled by a factor three before being written to data storage. This trigger scheme was in fact primarily optimized for studying inclusive  $e^+e^-$  production [3]. To

allow for trigger bias studies also LVL1 events requiring only two charged particles were recorded during part of the experiment. The LVL1 triggered on p+Nb reactions with 56% efficiency in the  $N_{ch} \geq 3$  mode and 72% efficiency in the  $N_{ch} \geq 2$  mode. These efficiencies correspond to the fraction of reactions that actually fired the LVL1 trigger. In total  $4.6 \times 10^9$  events – downsampled LVL1 or LVL2 – were recorded, corresponding to  $7.7 \times 10^9$  inspected LVL1 events and  $1.3 \times 10^{10}$  reactions in the target.

To study neutral-meson production the off-line data analysis searched for events containing four lepton tracks from which the 4-momentum of  $\pi^0$  and  $\eta$  mesons was fully reconstructed. Indeed, the electromagnetic decays of the latter, that is mostly  $\pi^0, \eta \rightarrow \gamma e^+ e^-$  (Dalitz) and  $\pi^0, \eta \rightarrow \gamma \gamma$ , combined with the external conversion of the decay photon(s) on material in the inner region of the HADES detector lead to events with a characteristic 4-lepton signature, namely  $\pi^0, \eta \rightarrow e^+ e^- e^+ e^-$ . Simulations show that the Dalitz decay contributes 25% (30%) of the detectable  $\pi^0$  ( $\eta$ ) yield. The direct branching into  $e^+ e^- e^+ e^-$  due to the decay into two virtual photons ( $\pi^0, \eta \rightarrow \gamma^* \gamma^*$ ) is however very small [27] and contributes in our case only about 2 – 2.5% of the total yield. Electron and positron tracks were identified following the procedures described in detail in [4, 26]. As no dedicated start detector was present in this experimental run, the start time for the time-of-flight measurement was reconstructed event-by-event from the most optimal assignment of different particle hypotheses ( $e^-$  or  $\pi^-$ ) to tracks of negatively charged fast particles. In the extraction of the inclusive negative pion yields no direct use was however made of the time-of-flight information, and the pion identification was solely based on energy-loss vs. momentum cuts (for details see [25]). Positive pions were identified likewise but, their spectra being partially contaminated by the much more abundant protons, they were not analyzed further.

### III. THE PHOTON-CONVERSION METHOD

The detection of high-energy photons via a full reconstruction of conversion pairs has been applied with success by the PHENIX [23] and ALICE [24] collaborations in ultrarelativistic collisions. Although those experiments comprise also electromagnetic calorimeters for photon detection, this alternative method is considered to offer valuable supplementary information on thermal photon as well as neutral-meson production. As HADES is presently not equipped with such a calorimeter, the conversion method opens a unique approach to  $\pi^0$  and  $\eta$  detection.

Meson reconstruction was realized with identified lepton tracks by joining opposite-sign leptons into  $e^+ e^-$  pairs and by further combining those dileptons pairwise into  $e^+ e^- e^+ e^-$  multiplets. Calculating the four-lepton invariant mass  $M_{e^+ e^- e^+ e^-}$  and setting appropriate

mass cuts allows to select the  $\pi^0$  and  $\eta$  mesons, respectively. Various opening angle cuts, optimized in extensive Monte-Carlo simulations, were applied to suppress combinations of uncorrelated leptons, namely  $\theta_{e^+ e^-} < 2.5^\circ$  on the dilepton with the smaller opening angle and  $\theta_{e^+ e^-} < 20^\circ$  on the second one (all angles given in the laboratory system). The  $2.5^\circ$  selection is optimal for conversion pairs while the  $20^\circ$  cut accepts also the more massive and hence wider Dalitz pairs. In addition, a cut was applied on the relative angle between the two dileptons in a multiplet, namely  $\theta_{\gamma^* \gamma^*} > 5^\circ$ , to suppress spurious counts at low  $M_{e^+ e^- e^+ e^-}$ . These cuts were adjusted on the data in order to maximize the meson yield while keeping the background of uncorrelated combinations low.

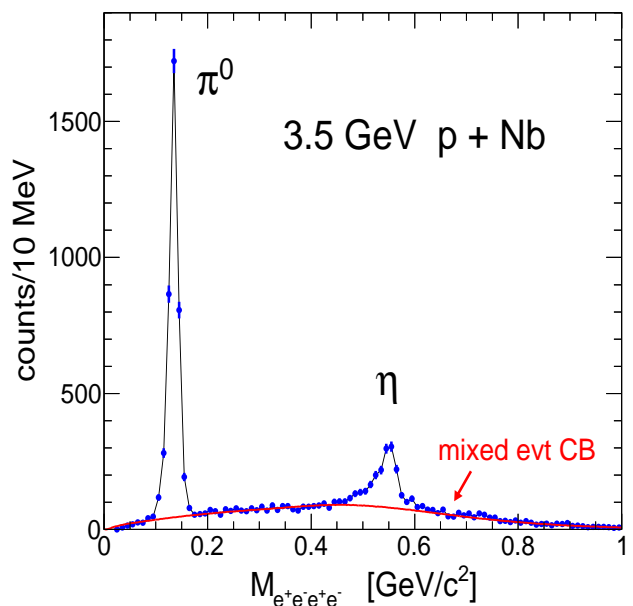


Figure 1: (Color online) Invariant-mass distribution of all  $e^+ e^- e^+ e^-$  multiplets (dots, error bars are statistical) measured with HADES in the 3.5 GeV p+Nb reaction. To improve visibility, the data points are connected by a thin curve. The background of uncorrelated lepton combinations obtained from event mixing is shown as well (solid curve).

The resulting  $M_{e^+ e^- e^+ e^-}$  distribution is shown in Fig. 1. Prominent peaks appear at the masses of the  $\pi^0$  and the  $\eta$  mesons on top of a continuum yield attributable to combinations of uncorrelated leptons. A systematic investigation of this combinatorial background (CB) was done, both by comparing the mass distributions of various charge combinations other than  $++$  and  $--$  and by applying an event mixing technique. We find that the largest part ( $> 90\%$ ) of the CB originates from the combination of uncorrelated dileptons, that is uncorrelated photons (real or virtual), mostly from multi- $\pi^0$  events. In that sense, the  $e^+ e^- e^+ e^-$  CB behaves very much like the two-photon CB observed in a calorimeter and it can hence be determined by event mixing. Thus, after subtraction of a mixed event CB normalized in the

Table I: Characteristics of the reconstructed meson peaks: raw signal counts above CB (integrated in the range 0.10 – 0.16 GeV/ $c^2$  for  $\pi^0$  and 0.46 – 0.60 GeV/ $c^2$  for  $\eta$ ), signal/CB ratio in those mass ranges, position of the peak maximum, and  $\sigma$  width of the peak ( $\sigma = \text{FWHM}/2.35$ ). All errors are statistical.

identified meson	$\pi^0$	$\eta$
signal [counts]	$3800 \pm 63$	$1240 \pm 49$
signal/CB	18.1	1.1
position [MeV]	$134 \pm 1$	$547 \pm 2$
width [MeV]	$8.0 \pm 0.6$	$19 \pm 2$

peak-free regions of the mass spectrum, the  $\pi^0$  and  $\eta$  peak characteristics are straightforwardly extracted. Integrated raw yields, peak positions and widths (defined as  $\sigma = \text{FWHM}/2.35$ ) are listed in Table I. Systematic errors on the yields from CB subtraction, estimated by varying the weights of the two normalization regions 0.2–0.4 and 0.6–1.0 GeV/ $c^2$ , are 5% for the  $\pi^0$  and 10% for the  $\eta$ , respectively. Having corrected the individual lepton momenta for their energy loss of typically 2–3 MeV, both peak positions are found to be consistent with the nominal meson masses, namely  $M_{\pi^0} = 0.13498$  GeV/ $c^2$  and  $M_{\eta} = 0.54785$  GeV/ $c^2$  [27]. The peak widths are determined by the momentum resolution of the HADES tracking system and the low-mass tails are partly due to lepton energy loss by bremsstrahlung. The overall mass resolution is comparable to the one achieved typically with electromagnetic calorimeters. Finally, from the observed yields inclusive meson multiplicities can be determined by correcting for acceptance and efficiency effects.

Note also that the  $\eta \rightarrow \pi^+\pi^-\pi^0$  and  $\eta \rightarrow 3\pi^0$  decays contribute to inclusive pion production. The latter of these two decay modes results in six final-state photons of which any combination of two can contribute via conversion to the measured  $e^+e^-e^+e^-$  signal. We have checked in simulations that these correlated lepton combinations lead to a broad structure in the  $M_{e^+e^-e^+e^-}$  invariant-mass distribution. Considering that the eta is a factor 20 less abundant than the pion (see Sec. IV) it is not surprising that this contribution is indistinguishable from the uncorrelated CB in Fig. 1.

We have performed extensive detector simulations to study the reconstruction efficiency of the conversion technique. To do this we have generated meson distributions with the Pluto event generator [28], tracked the resulting particles through a realistic model of the HADES setup with the GEANT3 physics simulation tool [29], embedded those tracks into real events from the p+Nb experiment, and reconstructed the overlayed events with the full HADES lepton analysis. The purpose of the embedding was to include realistic detector noise into the procedure. As the lepton identification in HADES relies

Table II: Average conversion probabilities  $\langle P_{conv} \rangle$  of decay photons in various inner parts of the HADES setup obtained from GEANT3 simulations. The last row gives the cumulated probability due to all materials contributing to the detection of  $\pi^0$  and  $\eta$  mesons. See text for a discussion of systematic uncertainties on those numbers.

Material	$\langle P_{conv} \rangle(\pi^0)$	$\langle P_{conv} \rangle(\eta)$
target (Nb)	2.17%	2.54%
target holder (C)	0.12%	0.14%
beam pipe (C)	0.46%	0.51%
radiator (C <sub>4</sub> F <sub>10</sub> )	0.79%	0.92%
cumulated	3.53%	4.11%

primarily on the RICH detector, only conversion pairs produced in the inner parts of the setup can contribute to the  $e^+e^-e^+e^-$  signal. These are the niobium target segments, the carbon-composite target holder, the carbon-composite beam pipe, and the RICH radiator gas C<sub>4</sub>F<sub>10</sub>. Conversion pairs produced in the RICH mirror or in any of the following materials are not detectable. Average conversion probabilities  $\langle P_{conv} \rangle$  of  $\pi^0$  and  $\eta$  decay photons obtained from the simulations are listed in Table II. More than half of the conversion takes place in the niobium targets and the rest in the target holder, the beam pipe, and the RICH converter gas, with a the cumulated probability of 3.5–4.1% per photon. The difference in probabilities for  $\pi^0$  and  $\eta$ , respectively, is related to the energy dependence of the conversion process. As the HADES pair vertex resolution, of the order of 2–3 cm, is not good enough to cleanly isolate the various converter parts in the event reconstruction we have refrained from applying specific vertex cuts and have exploited the cumulated conversion effect.

Systematic errors on the total conversion probability result mainly from uncertainties on the material budget and the alignment of the relevant inner detector parts. The thickness of the target foils is known with an error of 2% and their misalignment in the beam pipe adds an-

Table III: Average effective branching ratios  $\langle BR_{eeee} \rangle$ , geometric acceptances with respect to  $4\pi$   $\langle acc \rangle$ , pair reconstruction efficiencies  $\langle eff \rangle$ , and total detection efficiencies  $\langle eff_{tot} \rangle$  relevant for the reconstruction of the  $\pi^0, \eta \rightarrow e^+e^-e^+e^-$  final states. Statistical errors due to the finite size of the simulated sample are of the order of 3% for  $\pi^0$  and 2% for  $\eta$  on all listed quantities. Systematic uncertainties are discussed in the text.

Particle	$\langle BR_{eeee} \rangle$	$\langle acc \rangle$	$\langle eff \rangle$	$\langle eff_{tot} \rangle$
$\pi^0$	$1.68 \times 10^{-3}$	$4.53 \times 10^{-3}$	0.063	$4.78 \times 10^{-7}$
$\eta$	$9.72 \times 10^{-4}$	$2.87 \times 10^{-2}$	0.11	$3.03 \times 10^{-6}$

other 4% error. Inhomogeneities of the carbon-composite material lead to an estimated uncertainty of 10% on the holder and pipe contributions. Finally, for the radiator contribution we assume a 5% error. This leads then to an overall systematic error on the total material budget of 5% and hence an error of about 10% on the efficiency for detecting double conversion events.

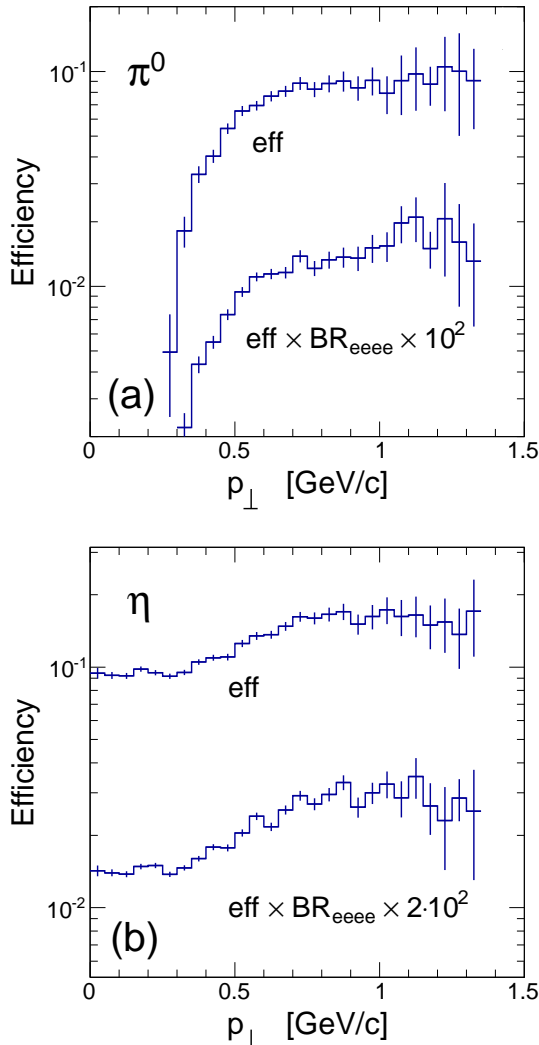


Figure 2: Efficiencies of meson reconstruction from  $e^+e^-e^+e^-$  events as a function of transverse momentum  $p_\perp$ . Shown are the  $\pi^0$  (a) and  $\eta$  (b) efficiencies with ( $eff \times BR_{eeee}$ ) and without ( $eff$ ) the contribution of the photon conversion. Error bars are statistical.

As we do not apply a secondary vertex selection to the  $e^+e^-$  pairs also Dalitz decays are included in our pair signal. In the Dalitz case, of course, only the one real photon is required to convert. The combined branching into all contributing final states ( $\gamma\gamma$ ,  $\gamma\gamma^*$ , and  $\gamma^*\gamma^*$ ) amounts to  $\simeq 100\%$  for the  $\pi^0$  and to  $\simeq 40\%$  for the  $\eta$  [27].

The meson sources used in the simulation were mod-

eled according to a fireball [30, 31] characterized by a temperature in the range  $T = 80\text{--}90$  MeV and a central laboratory rapidity in the range  $y_{max} = 0.92\text{--}0.96$ . As discussed below, the choice of these values is motivated by the data itself (cf. also Figs. 4 and 5). The Monte Carlo shows that the total detection efficiency  $eff_{tot}$  depends only weakly on the meson source properties and mostly on the photon conversion probability, on the geometric detector acceptance with respect to  $4\pi$  *acc*, and on the pair reconstruction efficiency  $eff$ . In this definition, *acc* includes the lepton low-momentum cutoff at around 50 MeV due to the track bending in the HADES magnet field and *eff* accounts for all detection and reconstruction losses within the HADES acceptance. As all of these quantities are averaged over the two-photon, the Dalitz, and the small direct decay channels it is useful to introduce an effective branching ratio  $BR_{eeee}$  into the  $e^+e^-e^+e^-$  final state which includes the photon conversion probability. Table III summarizes the result of our  $\pi^0 \rightarrow e^+e^-e^+e^-$  and  $\eta \rightarrow e^+e^-e^+e^-$  event simulations showing in particular that the total detection efficiencies are of order  $10^{-7} - 10^{-6}$ .

Systematic errors on the simulated efficiencies result from the uncertainties on the conversion probabilities (5% on  $P_{conv}$ , 7.5% on  $BR_{eeee}$ ), on the branching ratios of the contributing decays (1% on  $BR_{eeee}$  for  $\pi^0$  and 2% for  $\eta$ , from [27]), and on the detector and reconstruction efficiencies (10%, from a comparison of various simulated and measured observables in the HADES detector [26]). Combining all of these contributions we assign to the total efficiency a conservative systematic error of 15%.

The transverse momentum ( $p_\perp$ ) dependence of the meson reconstruction efficiency is depicted in Fig. 2, with and without the photon conversion probability included. The cutoff of the  $\pi^0$  efficiency at  $p_\perp \lesssim 0.35$  GeV/c is caused mostly by the strong bending of low-momentum tracks, i.e. those with  $p < 0.1$  GeV/c, in the HADES magnetic field. Because of the large mass of the eta meson, its efficiency is much less afflicted by low-momentum tracks and consequently reconstruction is possible down to zero  $p_\perp$ .

## IV. MESON YIELDS

### A. Negative pions

As pointed out above, besides measuring  $e^+$  and  $e^-$ , the HADES detector also provides high-quality data on charged hadrons. Here we use the concurrently measured negative pions [25] to validate the reconstructed  $\pi^0$  yields and extrapolate them to  $p_\perp < 0.35$  GeV/c. Figure 3 shows efficiency-corrected<sup>1</sup> double differential

<sup>1</sup> The  $\pi^-$  yields are corrected as well for the gaps caused in the azimuthal acceptance by the HADES magnet coils.

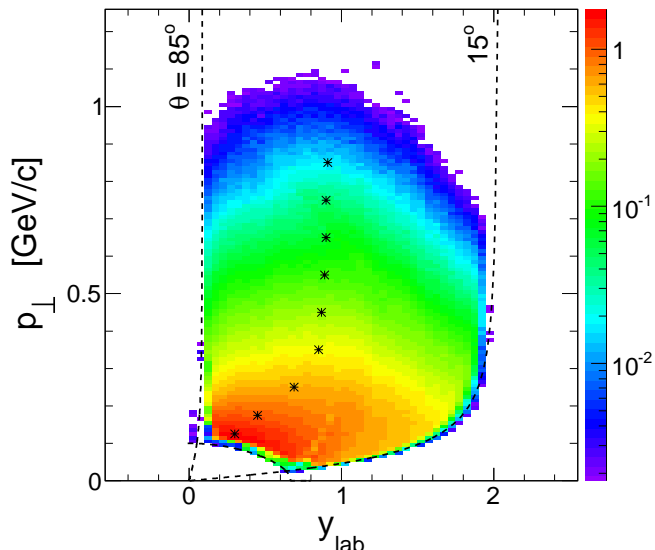


Figure 3: (Color online) Efficiency-corrected  $d^2N/dy dp_\perp$  distribution of negative pions detected by HADES in the 3.5 GeV p+Nb reaction. The color scale indicates yield per unit rapidity, per GeV, and per minimum-bias event. The dashed lines delineate the geometric acceptance (including a  $p > 0.12$  GeV/c cut), and the stars indicate loci of the maximum of the  $dN/dy$  distribution,  $y_{max}$ , as function of transverse momentum.

$\pi^-$  yields  $d^2N/dy dp_\perp$  adapted from [25]. The charged pion acceptance is constrained geometrically to polar angles of  $15^\circ - 85^\circ$  as well as by a momentum cut of  $p > 0.12$  GeV/c. This results in an acceptance in laboratory rapidity of  $y_{lab} \simeq 0.2 - 1.8$  and in transverse momentum of  $p_\perp \gtrsim 0.1$  GeV/c. Because of this quite large coverage one can expect that the extrapolation to full phase space will lead to moderate systematic uncertainties only. At a bombarding energy of 3.5 GeV the rapidity of the nucleon-nucleon center-of-mass system is at  $y_{NN} = 1.12$ . From the Fig. 3 it is however apparent that in the p+Nb reaction the pion yield is not peaked at a mid-rapidity  $y_{NN}$  but at a lower value with, in addition, a marked  $p_\perp$  dependence. Fits of a Gaussian function to  $dN/dy$  projections done for various  $p_\perp$  slices give the loci  $y_{max}$  of the maximum yield vs.  $p_\perp$ , as shown by stars in Fig. 3. In particular, low- $p_\perp$  pions seem to be radiated mostly from a target-like source, near  $y = 0$ , pointing to a high degree of stopping of the incoming projectile. Obviously not only first-chance nucleon-nucleon collisions contribute to pion emission in the p+Nb reaction, but proton elastic and inelastic rescattering followed by secondary production processes add a soft target-like component. This is also corroborated by various transport-model calculations [9, 11, 13].

Integrating  $d^2N/dy dp_\perp$  within the HADES rapidity coverage we find an accepted  $\pi^-$  yield of 0.50 per LVL1 event. From simulations we know that the LVL1 trigger leads to a 42% enhancement of the average detected

charged-pion yield per event (see [25]). Correcting for this trigger bias we obtain an accepted yield of 0.35 per p+Nb reaction. The Gauss fits done to the  $dN/dy$  projections provide furthermore a means to extrapolate the measured  $\pi^-$  yield outside of the HADES rapidity coverage. Alternatively, transport models, e.g. HSD [8], UrQMD [11], or GiBUU [13] (see Sec. V below), can be used to perform the extrapolation in  $y$  and  $p_\perp$  to full solid angle. In fact, integrating the yield within the geometric acceptance limits, extrapolating it either way — via Gauss fits to  $dN/dy$  projections in  $p_\perp$  slices or, better, with the help of transport calculations done for p+Nb — and correcting for the LVL1 bias we obtain on average a minimum-bias inclusive  $\pi^-$  multiplicity of  $N_{\pi^-} = 0.60$ . The error on this corrected  $\pi^-$  multiplicity is dominated by systematic effects introduced mostly by the correction of the LVL1 trigger bias ( $\pm 13\%$ ) and the spread in the model-dependent extrapolation in phase space ( $-10\%$ ,  $+15\%$ ); statistical errors are however negligible. Table IV lists the extracted multiplicity values and their associated uncertainties.

## B. Neutral mesons

We come now to the presentation of our differential  $\pi^0$  and  $\eta$  yields. First notice that the LVL1 trigger (meaning at least three charged hits in the TOF wall) does not introduce a bias on events with an  $e^+e^-e^+e^-$  signature. Likewise, the LVL2 trigger efficiency is found to be  $> 99\%$  for such events. Hence no explicit corrections for trigger effects are needed. The systematic uncertainties on the  $e^+e^-e^+e^-$  observables to be taken into account are those introduced by the efficiency correction ( $\pm 15\%$ ), the CB subtraction ( $\pi^0$ :  $\pm 5\%$ ,  $\eta$ :  $\pm 10\%$ ), and the model-dependent extrapolation to full solid angle ( $\pi^0$ :  $\pm 15\%$ ,  $\eta$ :  $\pm 10\%$ ).

As is visible from the invariant-mass spectrum in Fig. 1, both neutral mesons can be selected with appropriate mass cuts. We have used  $0.10 < M < 0.16$  for the  $\pi^0$  and  $0.46 < M < 0.60$  for the  $\eta$ . Subtracting the corresponding combinatorial background and applying corrections for photon conversion, as well as for lepton track identification and reconstruction efficiencies the double-differential yields  $d^2N/dy dp_\perp$  are obtained as a function of rapidity and transverse momentum. As stated in Sec. III, our efficiency corrections are based on the reconstruction of simulated meson decays embedded into real events. To do a first correction, we started out with relativistic Boltzmann distributions of an assumed temperature of 100 MeV and then refined this value in a second pass. The same holds for the central rapidities of the  $\pi^0$  and  $\eta$  sources which, like in case of the  $\pi^-$ , are observed to be substantially below the  $y_{NN} = 1.12$  value. All corrections were furthermore done concurrently in two dimensions,  $y$  and  $p_\perp$ , in order to alleviate any remaining dependence on our assumptions about the meson source characteristics. The resulting final  $dN/dp_\perp$



Table IV: Integrated minimum-bias inclusive meson multiplicities per p+Nb collision  $N_{acc}$ , within the accepted rapidity range  $0.2 < y_{lab} < 1.8$ , and  $N_{4\pi}$ , extrapolated to full solid angle. Statistical and systematic uncertainties are given; statistical errors are negligibly small for  $\pi^-$ .

Particle	$N_{acc}$	$N_{4\pi}$
$\pi^-$	$0.35 \pm 0.05$ ( <i>sys</i> )	$0.60 \pm 0.10$ ( <i>sys</i> )
$\pi^0$	$0.39 \pm 0.06$ ( <i>stat</i> ) $\pm 0.08$ ( <i>sys</i> )	$0.66 \pm 0.09$ ( <i>stat</i> ) $\pm 0.17$ ( <i>sys</i> )
$\eta$	$0.031 \pm 0.002$ ( <i>stat</i> ) $\pm 0.007$ ( <i>sys</i> )	$0.034 \pm 0.002$ ( <i>stat</i> ) $\pm 0.008$ ( <i>sys</i> )

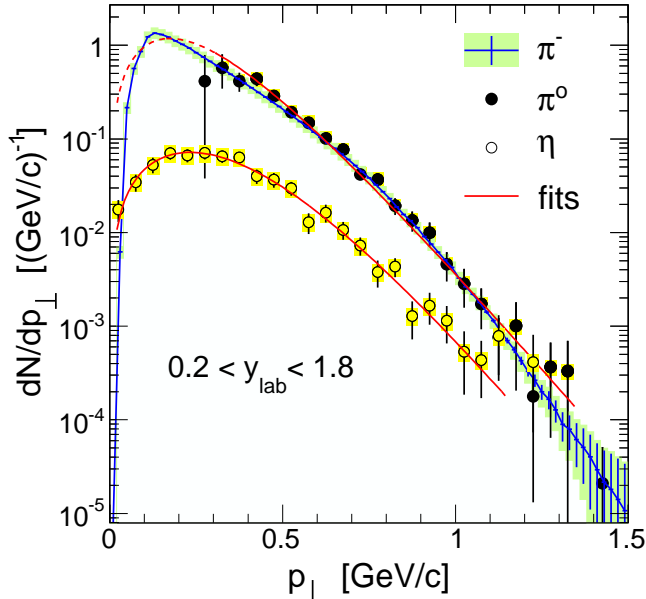


Figure 4: (Color online)  $\pi^0$  (full circles),  $\pi^-$  (blue histogram), and  $\eta$  (open circles) transverse momentum distributions  $dN/dp_\perp$  per minimum-bias event in 3.5 GeV p+Nb reactions within the HADES rapidity and momentum acceptance. The latter leads to a  $p_\perp \gtrsim 0.35$  GeV/c cut for the  $\pi^0$ . Statistical errors are shown as vertical bars, systematic errors as yellow and green shaded boxes. The red solid curves are Boltzmann fits to the  $\pi^0$  and  $\eta$  data (see text for details).

and  $dN/dy$  distributions, normalized per minimum-bias event, are displayed in Figs. 4 and 5. For comparison, the negative pion distributions are also shown.

Due to the efficiency cutoff discussed in Sec. III, no  $\pi^0$  yield is detected at low  $p_\perp$ . This is directly visible in Fig. 4 and it is also the reason why in Fig. 5 we show both pion rapidity distributions (i.e.  $\pi^0$  and  $\pi^-$ ) for  $p_\perp$  larger than 0.35 GeV/c only. For the  $\eta$  meson, however, the  $p_\perp$  coverage is complete. The rapidity coverage of both neutral mesons is restricted to  $y_{lab} = 0.2 - 1.8$  by the detector geometry. In a first attempt to characterize the observed meson yields we confront them with the isotropic fireball model [30, 31]. Adjusting a Boltzmann

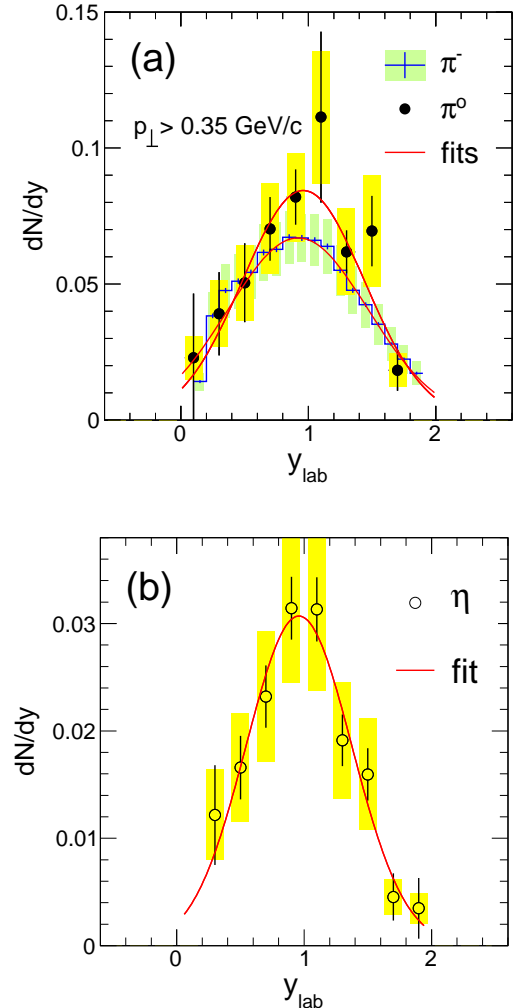


Figure 5: (Color online) (a)  $\pi^0$  (negative pion yield shown as histogram) and (b)  $\eta$  rapidity distributions  $dN/dy$  per minimum-bias event in 3.5 GeV p+Nb reactions. Pions are shown for  $p_\perp > 0.35$  GeV/c,  $\eta$  in full  $p_\perp$  range. Statistical errors are indicated by vertical bars, systematic errors are depicted by yellow shaded boxes. Red solid curves are Gauss fits to the data ( $\pi^0$ :  $y_{max} = 0.94 \pm 0.05$ ,  $\sigma_y = 0.48 \pm 0.06$ ,  $\chi^2/df = 6.1/6$ ;  $\pi^-$ :  $y_{max} = 0.91 \pm 0.01$ ,  $\sigma_y = 0.55 \pm 0.02$ ,  $\chi^2/df = 17.2/16$ ;  $\eta$ :  $y_{max} = 0.96 \pm 0.03$ ,  $\sigma_y = 0.41 \pm 0.03$ ,  $\chi^2/df = 5.2/6$ ).

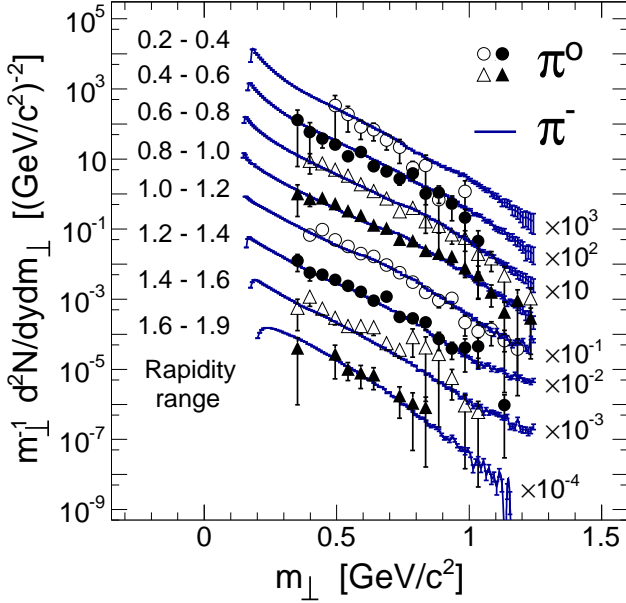


Figure 6: Transverse mass distributions per minimum-bias event  $m_{\perp}^{-1} dN/dm_{\perp}$  of measured  $\pi^{-}$  and  $\pi^0$  for the listed rapidity cuts. Error bars are statistical; systematic errors (not shown) on the  $\pi^{-}$  ( $\pi^0$ ) yields are  $\pm 13\%$  ( $\pm 19\%$ ).

type distribution  $dN/dp_{\perp} \propto p_{\perp} m_{\perp} K_1(m_{\perp}/T)$  to the meson transverse momentum distribution and a Gaussian  $dN/dy \propto \exp(-0.5(y - y_{max})^2/\sigma_y^2)$  to the rapidity distribution we find  $T = 92 \pm 3$  MeV ( $\chi^2/df = 17.4/18$ ),  $y_{max} = 0.94 \pm 0.05$ , and  $\sigma_y = 0.48 \pm 0.06$  ( $\chi^2/df = 6.1/6$ ) for the  $\pi^0$ , respectively  $T = 84 \pm 3$  MeV ( $\chi^2/df = 14.1/21$ ),  $y_{max} = 0.96 \pm 0.03$ , and  $\sigma_y = 0.41 \pm 0.03$  ( $\chi^2/df = 5.2/6$ ) for the  $\eta$ . Here  $K_1(x)$  is the modified Bessel function,  $m_{\perp} = \sqrt{p_{\perp}^2 + m^2}$  is the transverse mass,  $T$  is the fitted temperature parameter,  $y_{max}$  is the average source mid-rapidity (actually the peak position thereof), and  $\sigma_y$  is the width of the accepted rapidity distribution. The fit results show in particular that, within error bars, the rapidity distributions of both pion species agree in shape.

To characterize the pion source further, Fig. 6 shows the pion transverse-mass distributions  $m_{\perp}^{-1} dN/dm_{\perp}$  projected for various rapidity selections. It is apparent from this figure, and also Fig. 4, that a Boltzmann source does not describe very well the low- $p_{\perp}$  behavior. On the other hand, both pion species display in general a very similar behavior as function of  $m_{\perp}$  and  $y$ . Only in the first rapidity bin ( $y_{lab}=0.2 - 0.4$ ) the  $\pi^{-}$  show a somewhat harder spectrum than the  $\pi^0$ , which we attribute to a contamination of the  $\pi^{-}$  spectrum at small polar angles with fake tracks. We prefer, still, to use directly the

shape of the measured negative pion distribution<sup>2</sup> for extrapolating the  $\pi^0$  yield below 0.35 GeV/c. Doing this, we get a yield per minimum-bias event of  $N_{\pi^0} = 0.39$  within the accepted rapidity range of  $0.2 < y_{lab} < 1.8$ . In a second step the extrapolation to full solid angle can be done, based on transport-model calculations as discussed above, giving a minimum-bias inclusive multiplicity of  $N_{\pi^0} = 0.66$ . Statistical and systematic error bars on those results are given in Table IV.

For the eta meson, being four times heavier than the pion, the HADES detector provides complete transverse-momentum coverage. The rapidity coverage, although restricted to  $y_{lab} = 0.2 - 1.8$ , is very large too. Figures 4 and 5 show that the  $\eta$  phase space distribution is well described by a Boltzmann fit in transverse momentum and by a Gaussian in rapidity. The latter fit yields a width  $\sigma_y$ , which can be related [31] to the longitudinal temperature parameter  $T_{\parallel}$  of the eta source via the relation  $\sigma_y = \sqrt{T_{\parallel}/M_{\eta}}$ . From  $\sigma_y = 0.41 \pm 0.03$  and  $M_{\eta} = 0.548$  one obtains  $T_{\parallel} = 92 \pm 13$  MeV which is within error bars still consistent with the transverse temperature parameter obtained from the above Boltzmann fit, namely  $T = T_{\perp} = 84$  MeV. Finally, Fig. 7 shows Boltzmann fits to the  $\eta$  transverse mass distributions  $m_{\perp}^{-1} dN/dm_{\perp}$  for various rapidity selections, as well as the evolution with rapidity of the fitted slope parameter,  $T(y)$ . All of those are compatible with the assumption of an isotropic fireball: the  $m_{\perp}$  distributions are thermal with their slope varying like  $T_{\perp}/\cosh(y - y_{max})$  where  $T_{\perp}$  is taken from the previous Boltzmann fit to  $dN/dp_{\perp}$  and  $y_{max}$  is the central rapidity obtained in the above Gauss fit to  $dN/dy$ .

Integrating either of the  $dN/dy$  or  $dN/dp_{\perp}$  distributions we obtain a yield of 0.031 accepted eta per reaction and, extrapolating with the help of our fireball fits to full solid angle, an inclusive multiplicity of  $N_{\eta} = 0.034$ . Extrapolations based on transport models yield slightly larger values (see Sec. V). This is taken into account in the systematic uncertainties listed in Table IV.

Having available differential yields of both pions and etas from the same reaction, we can compare their scaling with transverse mass. So-called  $m_{\perp}$ -scaling has indeed been found previously for  $\pi^0$  and  $\eta$  production in 1 and 1.5 GeV/u Ar+Ca collisions [32]. The observation was that the production cross sections at mid-rapidity of different mesons are identical at a given  $m_{\perp}$  value. Model calculations have been able to reproduce this phenomenon [33, 34]. According to [33], in particular, proton-nucleus collisions should display  $m_{\perp}$ -scaling as well. In Fig. 8(a) we show, therefore, an overlay of our pion and eta  $m_{\perp}$  distributions for a few broad rapidity bins. We have chosen here the  $m_{\perp}^{-2} dN/dm_{\perp}$  representation, (i) because this form represents a Boltz-

<sup>2</sup> To do this the  $\pi^{-}$  spectrum was first corrected for its Coulomb shift  $E_C = -1.44(Z_{Nb} + 1)/R_{Nb} = -12$  MeV, where  $Z_{Nb} = 41$  and  $R_{Nb} = 5.2$  fm.



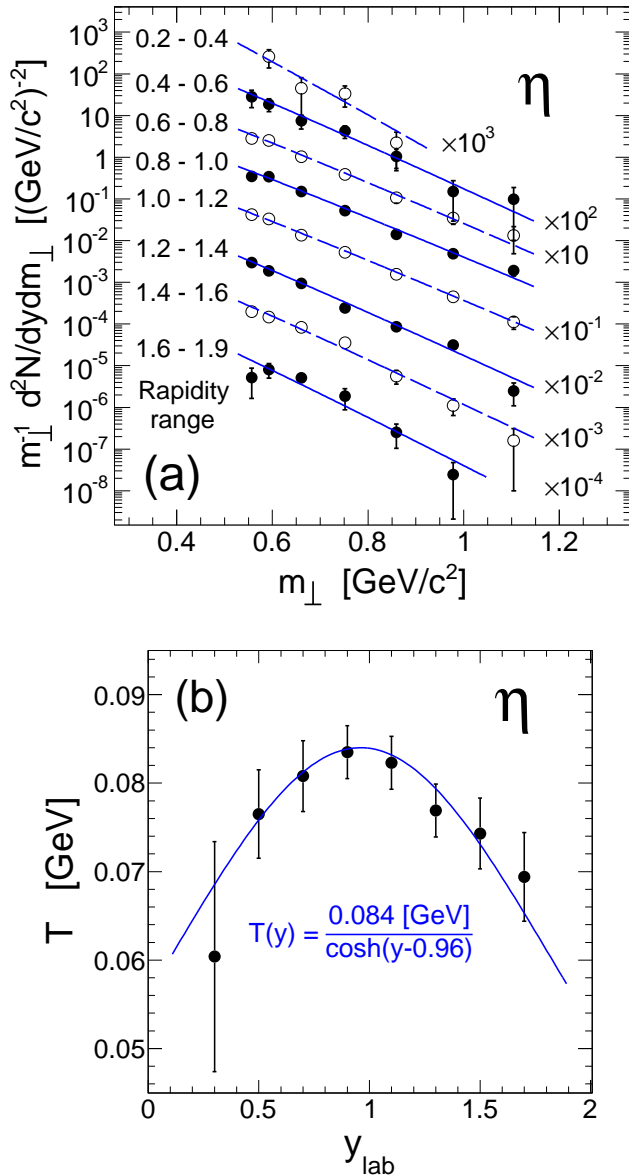


Figure 7: (a) Transverse mass distributions per minimum-bias event  $m_{\perp}^{-1} dN/dm_{\perp}$  of reconstructed eta mesons for the listed rapidity cuts. The data points have been corrected for their shift within the rather large  $m_{\perp}$  bins. Error bars shown are statistical only; systematic errors (not shown) on the yields are 21%. The curves are exponential fits to the data. (b) Resulting slope parameters  $T(y)$  shown as function of the rapidity. The solid curve corresponds to a thermal source of temperature  $T = 84$  MeV and central rapidity  $y_{\text{max}} = 0.96$ .

mann source as approximate exponential function, and (ii) because it is particularly well suited for visualizing  $m_{\perp}$ -scaling. Despite slight differences in slope — consistent with the temperature parameters obtained from the Boltzmann fits discussed above — an overall good agreement of the  $\pi^0$  and  $\eta$  yields at  $m_{\perp} > M_{\eta}$  is apparent. The  $\pi^-$  yields follow the  $m_{\perp}$ -scaling as well, except at low rapidities. As we discussed already in the context of Fig. 6, we attribute this deviation to a contamination of

fake tracks in the  $\pi^-$  spectrum. The same trends are visible in panel (b) of Fig. 8 which shows ratios of the meson yields, namely  $\pi^0/\pi^-$  and  $\eta/\pi^-$ . Except for part of the low-rapidity bin, the ratios are compatible with unity at transverse masses above  $M_{\eta}$ . We conclude that, albeit the pion spectra do not follow Boltzmann distributions at low transverse momentum,  $m_{\perp}$ -scaling seems to hold. This finding suggests that the meson yields are determined mostly by phase space: Although we can assume that meson production is mediated mostly by baryon resonance excitation, it does not matter whether one produces an eta meson at low momentum or a pion at high momentum, as long as their transverse mass is the same.

Finally, we want to point out that the extrapolated meson multiplicities can be transformed into a production cross section by multiplication with the total reaction cross section,  $\sigma_{\text{reac}}$ . Parameterizations of the proton-nucleus absorption cross section as function of bombarding energy do exist [35–37] and they suggest for p(3.5 GeV)+Nb values of  $\sigma_{\text{reac}}$  ranging from 990 mb (ref. [36]) to 1060 mb (ref. [37]). The comparison of  $\pi^-$  multiplicities measured with HADES and interpolated HARP  $\pi^-$  cross sections [16] yields a compatible value of  $\sigma_{\text{reac}} = 848 \pm 126$  mb [25].

## V. COMPARISON WITH TRANSPORT MODELS

Our observation that the rapidity distributions measured in the asymmetric p+Nb system are centered at values  $y_{\text{max}} < y_{NN}$  strongly suggests that, beyond first-chance nucleon-nucleon collisions, secondary reactions, i.e. processes involving multiple successive interactions of baryons and/or mesons contribute sizably to particle production. A similar behavior had already been noticed for kaon production in a previous study of p+Au collisions at comparable bombarding energies [38]. While the observed phase space population of the eta agrees quite well with a fireball description, this is questionable for the pion. Complete thermalization is apparently not reached in the p+Nb reaction and a transport-theoretical approach is required to model the complex interplay between reaction dynamics and particle production. Transport models typically handle meson and baryon production at energies up to a few GeV by resonance excitation and at higher energies through string fragmentation. In that respect, our beam energy is particularly challenging because it is situated in the transition region between these two regimes.

In the following we compare our results with three transport calculations done with either UrQMD, the Ultrarelativistic Quantum Molecular Dynamics model (version v3.3p1, see [11]), GiBUU, the Giessen Boltzmann-Uehling-Uhlenbeck model (version 1.5, see [13]), or HSD, the Hadron String Dynamics model (version 2.7, see [9]). At 3.5 GeV bombarding energy, corresponding to  $\sqrt{s_{NN}} = 3.18$  GeV, UrQMD runs in the resonance regime only

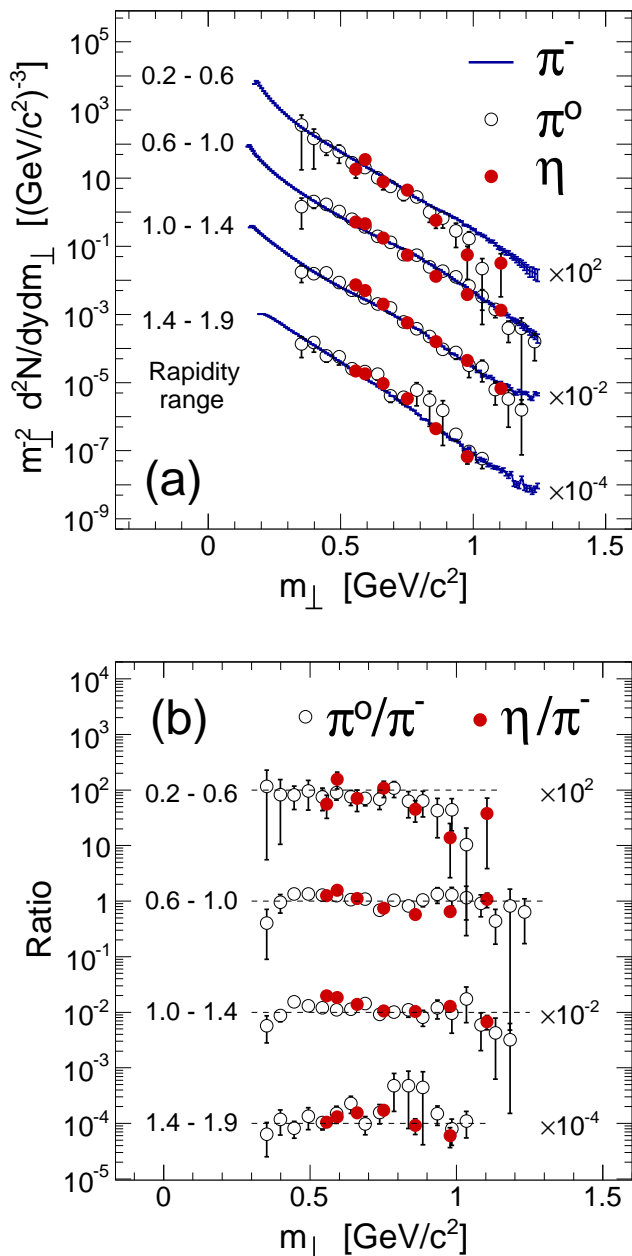


Figure 8: (Color online) (a) Illustration of meson  $m_{\perp}$ -scaling in 3.5 GeV p+Nb reactions by superimposing the reconstructed pion and eta transverse mass distributions,  $m_{\perp}^{-2}dN/dm_{\perp}$ . A bin-shift correction has been applied to the  $\eta$  data points. Four rapidity selections are shown; error bars are statistical only. (b) Yield ratios,  $\pi^0$  over  $\pi^-$  and  $\eta$  over  $\pi^-$ , as function of  $m_{\perp}$  for the same rapidity selections.

whereas HSD switches over to string fragmentation mode at  $\sqrt{s_{NN}} = 2.6$  GeV. For GiBUU, on the other hand, we present calculations done with two different realizations of this model: (i) the original implementation with a smooth transition to string fragmentation at  $\sqrt{s_{NN}} = 2.6$  GeV and (ii) a version (denoted hereafter by “ext. res.”) where the resonance region has been extended up

to about  $\sqrt{s_{NN}} = 3.5$  GeV [13].

Table V: Transport-model calculations of minimum-bias inclusive meson multiplicities per p+Nb collision,  $N_{\pi^0}$  and  $N_{\eta}$ , within the accepted rapidity range ( $0.2 < y_{lab} < 1.8$ ) as well as in the full solid angle ( $4\pi$ ).

Model	$N_{\pi^0}$		$N_{\eta}$	
	$0.2 < y < 1.8$	$4\pi$	$0.2 < y < 1.8$	$4\pi$
UrQMD v3.3p1	0.38	0.66	0.013	0.016
HSD v2.7	0.38	0.69	0.028	0.038
GiBUU v1.5	0.39	0.64	0.039	0.046
GiBUU ext res	0.32	0.49	0.031	0.034

Figure 9, panels (a) and (b), shows that  $\pi^0$  production is fairly well described by all models, and this in both observables  $p_{\perp}$  and  $y$ , within the HADES rapidity and transverse momentum acceptance. The pion yields reconstructed in the rapidity range  $y_{lab} = 0.2 - 1.8$  are in fact reproduced to within 10-25% (cf. Table IV vs. Table V). The rapidity distributions of all models are very similar with a slight tendency of being shifted towards target rapidity. Differences between the various calculations are mostly visible for  $p_{\perp} < 0.3$  GeV/c and for  $p_{\perp} > 1$  GeV/c. Notice also that at low  $p_{\perp}$  the standard implementation of GiBUU behaves more in line with UrQMD than the one with an extended resonance region. This is somewhat surprising as one would rather expect that this modification of GiBUU increases the similarity of the two models.

Comparing next in Fig. 9, panels (c) and (d), the calculated and measured  $\eta$  distributions, larger discrepancies between the models do appear. While UrQMD reproduces quite well the  $dN/dp_{\perp}$  shape, it underestimates the accepted yield by a factor of 2-3 and also misses the  $dN/dy$  shape. Both versions of GiBUU, on the other hand, do fairly well in describing the  $\eta$  rapidity distribution and integrated yield (see Table V), and its extended-resonance implementation also possesses the correct transverse-momentum behavior. The HSD pion and eta yields, finally, do agree fairly well with the data, albeit their  $y$  and  $p_{\perp}$  distributions deviate substantially. The complete lack of data in the energy range discussed here probably explains why the models tend to perform worse for  $\eta$  production than they do for pions. We are confident that with the help of our new results a more detailed theoretical investigation of the relevant production processes will now be possible.

## VI. SUMMARY

To summarize, we have presented data on inclusive pion and eta production in the reaction p+Nb at 3.5 GeV kinetic beam energy. In this study we have used the

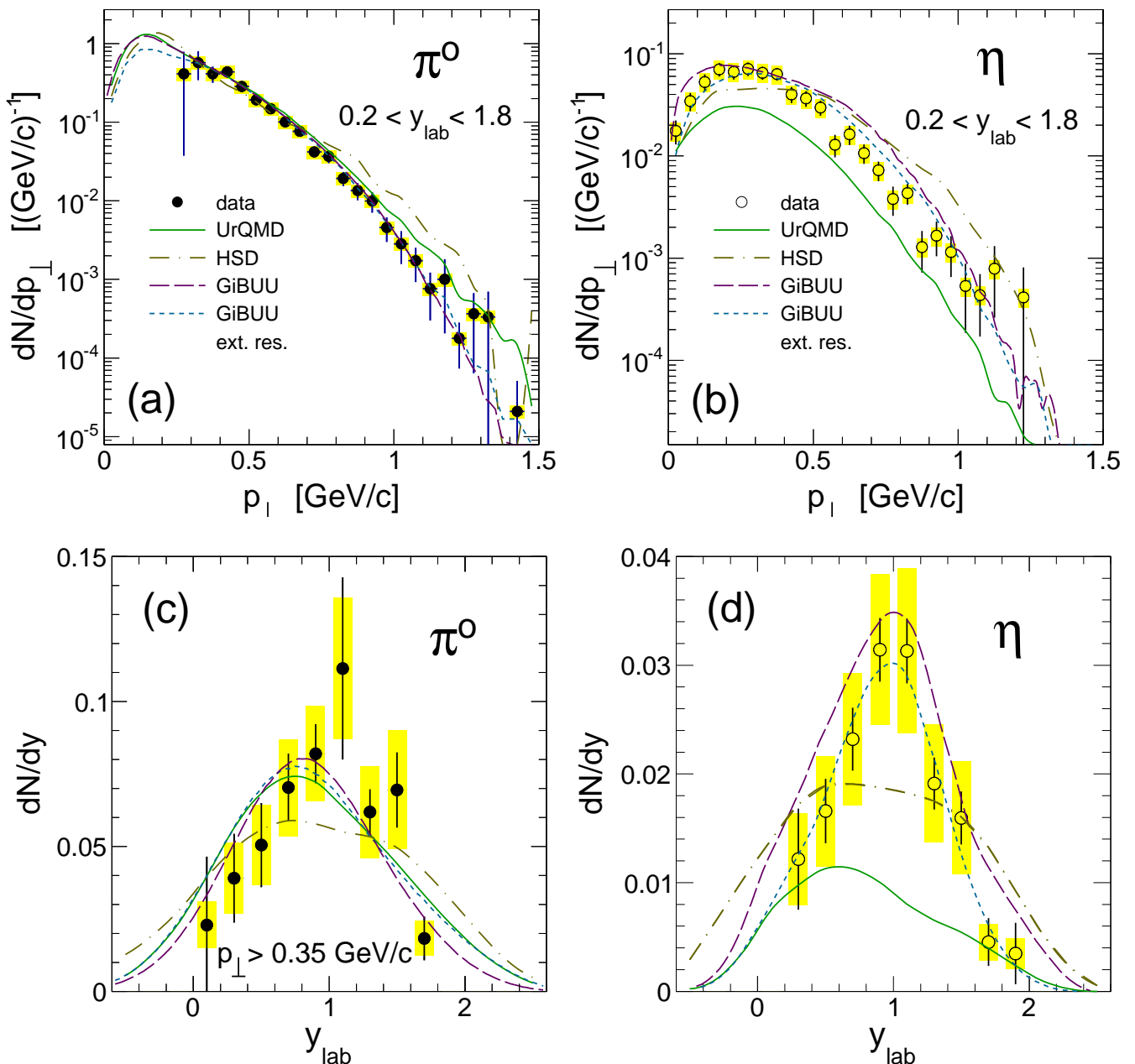


Figure 9: (Color online) (a)  $\pi^0$  and (b)  $\eta$  transverse momentum distributions  $dN/dp_{\perp}$  per minimum-bias event in 3.5 GeV p+Nb reactions (symbols) compared to results of the UrQMD, HSD, and GiBUU transport models. For the latter one, also the extended-resonance implementation is shown (see text). All error bars are as in Fig. 4. (c)  $\pi^0$  (with  $p_{\perp} > 0.35 \text{ GeV}/c$ ) and (d)  $\eta$  rapidity distributions  $dN/dy$  per minimum-bias event compared to transport calculations. The meaning of the lines is as in (a) and (b), error bars are as in Fig. 5.

photon-conversion method to detect and reconstruct neutral mesons from 4-lepton final states. We have demonstrated that with HADES quantitative results on differential  $\pi^0$  and  $\eta$  yields can be obtained over a large range of transverse momentum and rapidity. Our data provide valuable new input for the theoretical description of proton-nucleus and nucleus-nucleus collisions in the few-GeV energy regime with respect to both meson dy-

namics and dilepton emission. This is exemplified in our comparison with a selection of available transport models revealing an overall fair to good agreement in various observables. Together with our previous studies of p+p reactions [1, 2], the present results provide the required baseline for measurements with heavy-ion beams at the future FAIR facility. Indeed, as its central component — the SIS100 accelerator — is designed to provide intense

beams of even the heaviest ions up to 8 GeV/ $u$ , we will be in the position to isolate unambiguously those effects induced by the hot and dense baryonic medium.

### Acknowledgments

We thank E. Bratkovskaya and J. Weil for providing us with their latest HSD, respectively GiBUU, transport calculations. The HADES Collaboration

gratefully acknowledges the support by BMBF grants 06DR9059D, 05P12CRGHE, 06FY171, 06MT238 T5, and 06MT9156 TP5, by HGF VH-NG-330, by DFG EClust 153, by GSI TMKRUE, by the Hessian LOEWE initiative through HIC for FAIR (Germany), by EMMI GSI, by grant GA CR 13-067595 (Czech Rep.), by grant NN202198639 (Poland), by grant UCY-10.3.11.12 (Cyprus), by CNRS/IN2P3 (France), by INFN (Italy), and by EU contracts RII3-CT-2005-515876 and HP2 227431.

- 
- [1] G. Agakishiev *et al.* (HADES Collaboration), Phys. Rev. C **85**, 054005 (2012).
  - [2] G. Agakishiev *et al.* (HADES Collaboration), Eur. Phys. J. A **48**, 64 (2012).
  - [3] G. Agakishiev *et al.* (HADES Collaboration), Phys. Lett. B **715**, 304 (2012).
  - [4] G. Agakishiev *et al.* (HADES Collaboration), Phys. Rev. C **84**, 014902 (2011).
  - [5] S. Leupold, V. Metag, and U. Mosel, Int. J. Mod. Phys. E **19**, 147 (2010).
  - [6] R. S. Hayano and T. Hatsuda, Rev. Mod. Phys. **82**, 2949, (2010).
  - [7] R. Rapp and E. V. Shuryak, Phys. Lett. B **473**, 13 (2000); K. Gallmeister, B. Kämpfer, and O. P. Pavlenko, Phys. Rev. C **62**, 057901 (2000).
  - [8] E. L. Bratkovskaya and W. Cassing, Nucl. Phys. A **807**, 214 (2008).
  - [9] E. L. Bratkovskaya *et al.*, arXiv:1301.0786v3 [nucl-th], to appear in Phys. Rev. C.
  - [10] S. A. Bass *et al.*, Prog. Part. Nucl. Phys. **41**, 225 (1998).
  - [11] K. Schmidt *et al.*, Phys. Rev. C **79**, 064908 (2009).
  - [12] O. Buss *et al.*, Phys. Rep. **512**, 1 (2012).
  - [13] J. Weil *et al.*, Eur. Phys. J. A **48**, 111 (2012).
  - [14] S. Nagamiya *et al.*, Phys. Rev. C **24**, 971 (1981).
  - [15] N. J. DiGiacomo *et al.*, Phys. Rev. C **31**, 292 (1985).
  - [16] A. Bolshakova *et al.*, Eur. Phys. J. C **62**, 293 (2009); **63**, 549 (2009); **64**, 181 (2009); **66**, 57 (2009);
  - [17] E. Chiavassa *et al.*, Europhys. Lett. **41**, 365 (1998).
  - [18] V. Koreshev *et al.* (E672 and E706 Collaborations), Phys. Rev. Lett. **77**, 4294 (1996).
  - [19] T. Alexopoulos *et al.* (E771 Collaboration), Phys. Rev. D **62**, 032006 (2000).
  - [20] A. Abulencia *et al.* (CDF Collaboration), Phys. Rev. Lett. **98**, 232001 (2007).
  - [21] G. Aad *et al.* (ATLAS Collaboration), Phys. Rel. Lett. **108**, 152001 (2012).
  - [22] S. Chatrchyan *et al.* (CMS Collaboration), Eur. Phys. J. C **72**, 2251 (2012).
  - [23] T. Dahms *et al.* (PHENIX Collaboration), Eur. Phys. J. C **49**, 249 (2007).
  - [24] K. Koch *et al.* (ALICE Collaboration), Nucl. Phys. A **855**, 281 (2011).
  - [25] P. Thusty *et al.* (HADES Collaboration), Proceeding of the 50th International Winter Meeting on Nuclear Physics, Bormio (Italy) 2012, PoS (Bormio2012), 019.
  - [26] G. Agakishiev *et al.* (HADES Collaboration), Eur. Phys. J. A **41**, 243 (2009).
  - [27] J. Behringer *et al.* (Particle Data Group), Phys. Rev. D **86**, 010001 (2012).
  - [28] I. Fröhlich *et al.*, Proceedings of the 11th International Workshop on Advanced Computing and Analysis Techniques, Amsterdam (The Netherlands) 2007, PoS (ACAT) 076.
  - [29] GEANT 3.21, Detector description and simulation tool, CERN long writeup W5013 (1993).
  - [30] R. Hagedorn, Rivista del Nuovo Cimento **6**, 1 (1983).
  - [31] E. Schnedermann, J. Sollfrank, and U. Heinz, Phys. Rev. C **48**, 2462 (1993).
  - [32] F. D. Berg *et al.* (TAPS collaboration), Phys. Rev. Lett. **72**, 977 (1994).
  - [33] K. K. Gudima, M. Ploszajczak, V. D. Toneev, Phys. Lett. B **328**, 249 (1994).
  - [34] E. L. Bratkovskaya, W. Cassing, and U. Mosel, Phys. Lett. B **424**, 244 (1998).
  - [35] L. Sihver, C. H. Tsao, R. Silberberg, T. Kanai, and A. F. Barghouty, Phys. Rev. C **47**, 1225 (1993).
  - [36] R. K. Tripathi, F. A. Cucinotta, and J. W. Wilson, Nucl. Instr. Meth. Phys. Res. B **117**, 347 (1996).
  - [37] H. P. Wellisch and D. Axen, Phys. Rev. C **54**, 1329 (1996).
  - [38] W. Scheinast *et al.* (KaoS Collaboration), Phys. Rev. Lett. **96**, 072301 (2006).